Strongly Correlated Ion Coulomb Systems

Michael Drewsen, Anders Mortensen, Esben Nielsen and Thierry Matthey

QUANTOP - Danish National Research Foundation Centre for Quantum Optics
Department of Physics and Astronomy
University of Aarhus
Ny Munkegade Building 1520, DK-8000 Aarhus C, Denmark

Abstract. As a specific example of strongly correlated Coulomb systems, three-dimensional long-range ordered structures in smaller and near-spherically symmetric Coulomb crystals of $^{40}Ca^{+}$ ions confined in a linear rf Paul trap are discussed. Though the observed structures are not expected from ground state molecular dynamics (MD) simulations, similar structures are found as metastable ion configurations in MD simulations at low temperatures.

INTRODUCTION

Confined ensembles of particles with identical sign of charge interacting through the Coulomb force constitute an interesting class of long range interacting systems. Such systems, sometimes referred to as non-neutral plasmas (NNPs), have in the past particularly been investigated in the case of one component Plasmas (OCPs), i.e., NNPs consisting of identical particles. More specifically, so-called strongly coupled one component plasmas (SCOCPs), defined as OCPs where particle correlations are significant, have attracted much attention.

Theoretically, it has been found that the thermodynamic properties of infinite OCPs of a single species are fully characterized by the coupling parameter [1]

$$\Gamma = \frac{1}{4\pi\varepsilon_0}\frac{Q^2}{a_{ws}k_bT} \tag{1}$$

where Q is the charge of the particles, a_{ws} is the Wigner-Seitz radius defined from the zero temperature particle density n_0 by $n_0 = 3/4\pi a_{ws}^3$. Furthermore, a liquid-solid transition to a body centered cubic (*bcc*) structure is expected to occur for $\Gamma \sim 170$ [2, 3]. For finite OCPs the situation is more complex, and the properties will depend both on the size and shape of the ion plasma, since surface effects cannot be neglected [4, 5, 6, 7, 8].

Laser-cooled ion plasmas confined by electromagnetic fields in Penning traps [9, 10, 11] or in radio-frequency (rf) traps [12, 13, 14, 15, 16], have offered an excellent opportunity to study SCOCPs. Investigations of the solid structures, often referred to as Coulomb crystals, have ranged from one-dimensional (1D) long cylindrical crystals [12, 13, 14, 16] over 2D thin planar crystals [11] to 3D spheroidal crystals [9, 10, 11, 13]. Surface-effects in finite 3D spheroidal ion Coulomb crystals ha have been reported in Refs. [13, 14] where the structures were found to be composed of concentric ion shells.

CP970, *Dynamics and Thermodynamics of Systems with Long-range Interaction: Theory and Experiments*
edited by A. Campa, A. Giansanti, G. Morigi, and F. Sylos Labini

Simulations indicate that the ions are expected to form a near-2D hexagonal ordered structure within each shell in such cases [5].

Observations of three-dimensional long-range order associated with infinite systems were first reported in the case of ∼50 000 or more laser-cooled ions in a Penning trap [4,5,9]. Only recently similar structures have been observed in rf traps with nearly spherical symmetric Coulomb crystals ranging in size from ∼1000 – ∼20,000 ions [17].

In the present contribution we will focus on these latter observations and discuss the experimental results in relation to molecular dynamics (MD) simulations.

THE EXPERIMENTAL SETUP

The linear Paul trap used in the experiments is shown in Fig.1. Since it is described in detail elsewhere [24], we give here only a brief description of its basic properties. The linear Paul trap consists essentially of four circular electrode rods in a quadrupole configuration. Radial confinement of the ions is obtained by applying a sinusoidally time-varying rf potential $\frac{1}{2}U_{rf}\sin(\omega_{rf}t)$ to diagonally opposite electrodes and the same time-varying potential, but with a phase shift of π, to the two remaining electrode rods. Static axial confinement is achieved by having all electrode rods sectioned into three parts with the eight end-pieces kept at a positive dc potential U_{end} with respect to the four center pieces.

The electrode rod radius R is 2.0 mm, and the closest distance from the trap axis to the electrodes r_0 is 3.5 mm. Each sectioned rod has a 5.4 mm long center-piece ($2 \times x_0$) and 20.0 mm long end-pieces (x_{endcap}). The frequency of the rf field is in all experiments $\omega_{rf} = 2\pi \times 3.88$ MHz. With the definition given in Ref. [19] of the relevant stability parameters q and a for the linear Paul trap under the present operation conditions, the geometry of the trap leads to $q = 6.6 \times 10^{-4}U_{rf}$ [V] and $a = 5.5 \times 10^{-4}U_{end}$ (the voltages in units of Volts). In the experiments, the rf amplitude U_{rf} is maximally 500 V, corresponding to $q_{max} = 0.33$ This value is small enough that in all the experiments a harmonic pseudopotential with rotational symmetry with respect to the trap axis and a uniform zero temperature ion density given by $n_{theo} = \varepsilon_0 U_{rf}^2/(mr_0^4\omega_{rf}^2)$ can be assumed (ε_0 is the vacuum permittivity and m the mass of the ion). The $^{40}Ca^+$ ions used in the experiments are produced isotope selectively by resonance-enhanced photoionization of atoms from an effusive beam of naturally abundant calcium [20, 21]. Doppler laser cooling is achieved along the trap center axis by using counter-propagating laser beams tuned to the $4S_{1/2} - 4P_{1/2}$ transition at 397 nm and with a repumper beam on the $4D_{3/2} - 4P_{1/2}$ transition at 866 nm. The radial motion of the ions is cooled indirectly through the Coulomb coupling of the radial and axial degrees of freedom. Images of the ions in the trap are obtained by detecting the 397 nm light spontaneously emitted during the laser cooling process by a CCD camera equipped with an image intensifier and a 14× magnification lens system. As indicated in Fig. 2 (a), the imaging optic is situated such that the real crystal structure is projected to a plane including the trap axis. Because of the rotational symmetry of the Coulomb crystal boundary around the trap axis, we can deduce from the images their real 3D sizes and hence the number of ions by using the expression for the ion density given above. With an exposure time of 100 ms used in the experiments, the quadrupole deformations of the Coulomb crystal induced by the rf field

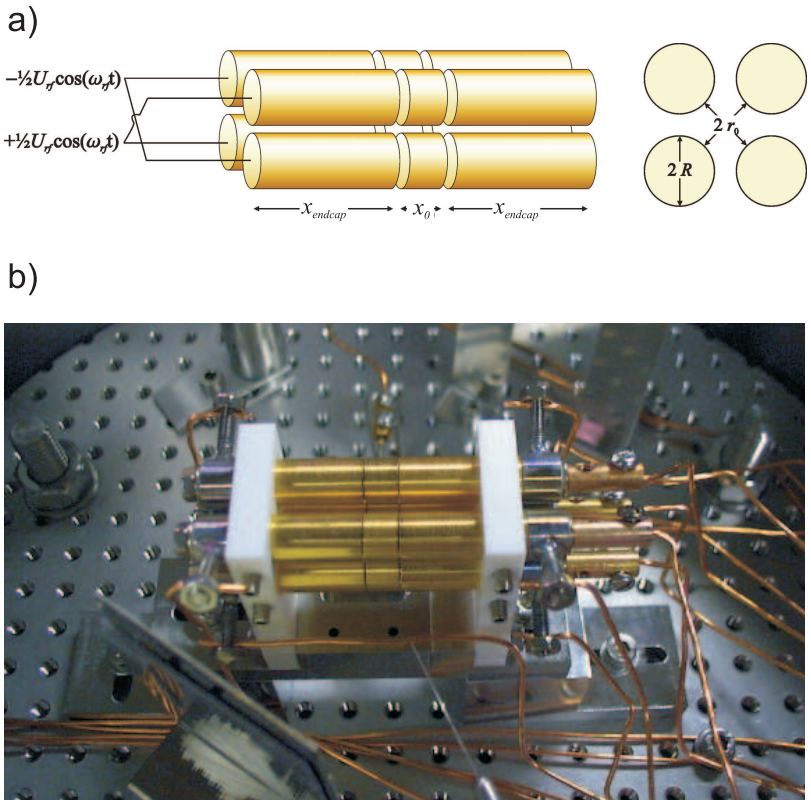

FIGURE 1. (a) Sketch of the linear trap used in the experiments. The various parameters are defined in the text. (b) Picture of the actual trap used. As a scale, the center-part of the electrode ($2 \times x_0$) is 5.4 mm. The figure is reproduced from Ref. [18]

are averaged out in the images. The direction of the micromotion [22] of the individual ions is position dependent as indicated in Fig. 2(a). As a result, only ions close to the horizontal trap plane defined by the horizontal dashed line in Fig. 2(a) and the trap axis are imaged without micromotion blurring due to their micromotion only being in the direction of view (DV) of the camera system.

OBSERVED COULOMB CRYSTAL STRUCTURES

In Fig. 2(b), an image of a slightly prolate ion Coulomb crystal consisting of about 2300 ions is presented. Clearly visible is a hexagonal structure. From a series of experiments where the position of the crystal along the z-axis is being changed, such hexagonal structures are also found present when imaging other regions of the crystal [17].

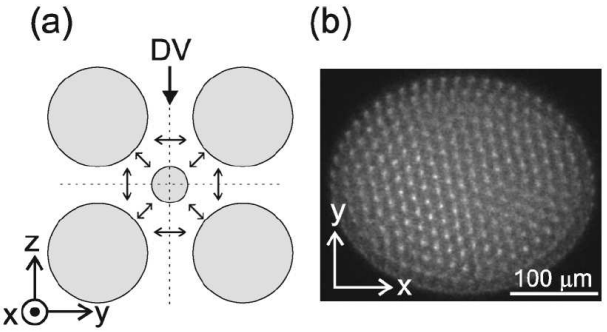

FIGURE 2. (a) The four main circles indicate the four cylindrical trap electrode rods viewed along the trap axis (*x*-axis). The small circle in the center represents a radially centered Coulomb crystal in the trap. The small double arrows indicate the positional dependent direction of the micromotion of the ions in the trap. The single arrow denotes the direction of view (DV) for the camera system. (b) Image of a Coulomb crystal consisting of ∼2300 ions. The figure is reproduced from Ref. [17]

From the pre-knowledge that the ground state of larger ion systems is a *bcc* configuration [2, 3], it is tempting to assume that the observed structure is indeed a *bcc* structure observed along the [111] direction. However, also simple cubic (*sc*) and face centered cubic (fcc) structures will lead to similar hexagonal patterns for the same direction of observation. For a specific side length d of the triangles making up the observed structure, the three cubic structures correspond fortunately to different ion densities related by $n_{bcc} = 2n_{sc} = 4n_{fcc} = 1.089/d^3$. The perfect agreement between the expected density of $n_{theo} = 2.3 \pm 0.2 \times 10^8 cm^{-3}$ with the one obtained from the images $n_{bcc} = 2.1 \pm 0.3 \times 10^8 cm^{-3}$, strongly supports that the observed structure is indeed a *bcc* and certainly not a *sc* or fcc structure. As long as the crystal is not too oblate or prolate, the outer shape of the crystal is not critical for observing the long-range structures, as can be seen in Figs. 3(a)-3(c).

A series of measurements on near spherical crystals with different numbers of ions were done to investigate the size effect of the observation of three-dimensional long-range structures. A few resulting images of this study are presented in Figs. 3(d)–3(f). Here one observes long-range-order for as few as 770 ions (Fig. 3(e)), and even some structure is present in the core for the case of 290 ions (Fig. 3(f)). When comparing the images in Fig. 3, it is evident that the relative number of ions in the regular structure decreases with the size of the crystals, as may be expected since the outer layer of the crystals is always spheroidal shaped. Another size dependent quantity noticed is the frequency at which ordered structures are being observed: the smaller the crystals the more unlikely it is to observe the regular structures. The rate at which the long-range ordered structures are observed in crystals of a few thousand ions is about 0.1 Hz and the lifetime of the structure is a few hundred ms. In all cases, since the exposure time of 100 ms is many orders of magnitude larger than both the rf period (∼ 250 ns) and the time scale of crystal vibrations ($\sim 1\mu s$), the crystal structures are at least to be considered as metastable states.

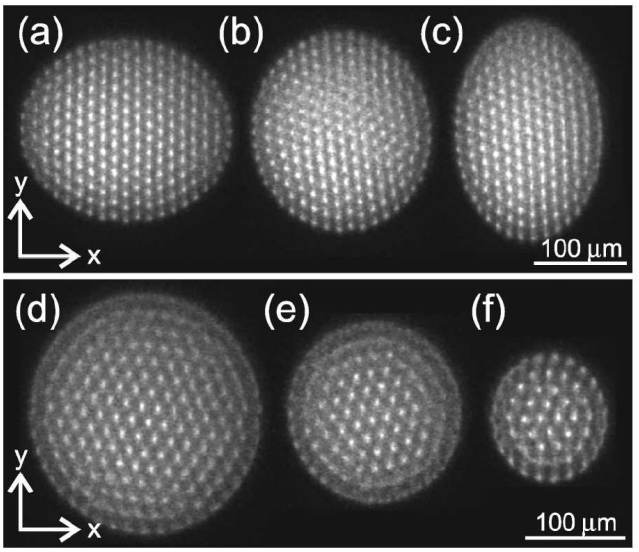

FIGURE 3. Images of Coulomb crystals. The first column shows three crystal images of the same $\sim$2000 ions with the trap potentials being $U_{rf} = 500$ V and (a) $U_{end} = 27$ V, (b) $U_{end} = 33$ V, and (c) $U_{end} = 40$ V, respectively. The second column represents images near spherical crystals for the same trap potentials $U_{rf} = 400$ V and $U_{end} = 21$ V. The number of ions in the crystals is (d) 1700, (e) 770, and (f) 290, respectively. The figure is reproduced from Ref. [17]

MD SIMULATION RESULTS

Molecular dynamics (MD) simulations of ground state configurations of Coulomb crystals in static spherical harmonic potentials have shown that only when the number of ions exceeds $\sim$5000 a pronounced *bcc* structure is expected [23, 24]. However, in contrast to ground state simulations, a certain thermal energy is always present in experiments, and configurations different from the ground state may occur. In order to understand the observed long-range-ordered structures, we have made several MD simulations using a static spherical harmonic potential where we initially kept a core of the ions fixed in a *bcc* structure and cooled the surrounding ions slowly until $\Gamma > 100,000$ was reached. For an ion system of $\sim$1000 ions, the excess potential energy (relative to the ground state configuration) of such artificially created cold configurations is even with more than one tenth of the ions kept fixed in a *bcc* structure several times smaller than the thermal energy of the system at the typical experimental temperature of a few mK. Simulations where all the ions were subsequently slowly heated to $\Gamma \sim 400$ (corresponding to a few mK) furthermore showed that the artificially created configurations could be metastable on the time scale of the exposure time of the images, $\sim$10 ms. Figure 4(a) is an example of a constructed image based on the results of a MD simulation of a crystal of 2685 ions heated to $\sim$400 (temperature: 5 mK), where initially 10% of the most centrally positioned ions were kept fixed in a *bcc* structure. With the 10 ms integration time of this

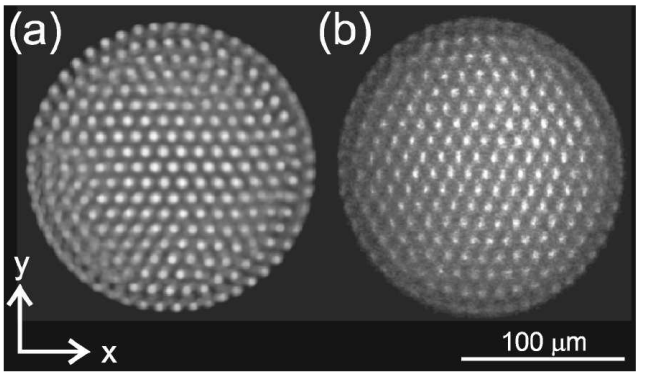

FIGURE 4. Images of Coulomb crystals. (a) Time averaged image based on data from MD simulations of Coulomb clusters with 2685 ions at $\Gamma \sim 400$ (temperature: $\sim$5 mK). The averaging time is 10 ms. (b) Image from experiments with clusters containing $\sim$ 2700 ions. The figure is reproduced from Ref. [17]

simulation, the central *bcc* structure is seen to be well preserved, and the image resembles very much the experimentally obtained image of a Coulomb crystal with about the same number of ions (Fig. 4(b)).

For crystals with more than $\sim$2000 ions, images are observed, which suggests three-dimensional long-range ordering different from *bcc*. In Fig. 5, images of the same ion ensemble ($\sim$13 000 ions) at two different instants are presented. While the hexagonal structure of Figs. 5(a) and 5(b) with $d = 17.2 \pm 0.8 \mu m$ again is compatible with a *bcc* structure, the rectangular structure observed in Figs. 5(c) and 5(d) cannot be interpreted as another projection of a *bcc* structure, but has to relate to another structure. The lengths of the sides of the rectangle are $h = 15.2 \pm 0.5 \mu m$ and $w = 9.7 \pm 0.2 \mu m$, respectively, which yields a ratio of the sides of $h/w = 1.55 \pm 0.06$. No projection of cubic crystal structures exactly complies with this ratio, but a fcc structure projected in the [211] direction has the ratio h/w = 1.63. For the expected ion density of $n_{theo} = 2.2 \pm 0.2 \times 10^8 cm^{-3}$, the corresponding side lengths of the projected rectangles should for a fcc structure have been $h = 15.2 \pm 0.5 \mu m$ and $w = 9.3 \pm 0.3 \mu m$, respectively. The origin of the small discrepancy between the observed and the predicted ratios is at present unknown, but an explanation could probably be found in a micromotion induced distortion of the fcc lattice. The observation of fcc structures is not so surprising since such structures have already been observed for larger near-spherical Coulomb crystals in Penning traps [10]. Furthermore, MD simulations have also predicted very small differences in the potential energies of *bcc* and fcc structures for larger crystals [24].

The reason why the observed *bcc* or fcc structures always seem to be observed from a specific direction is still not completely understood. However, the non-perfect cylindrical symmetry of the quadrupole trap configuration and the corresponding micromotion as well as small patch potentials may play a role.

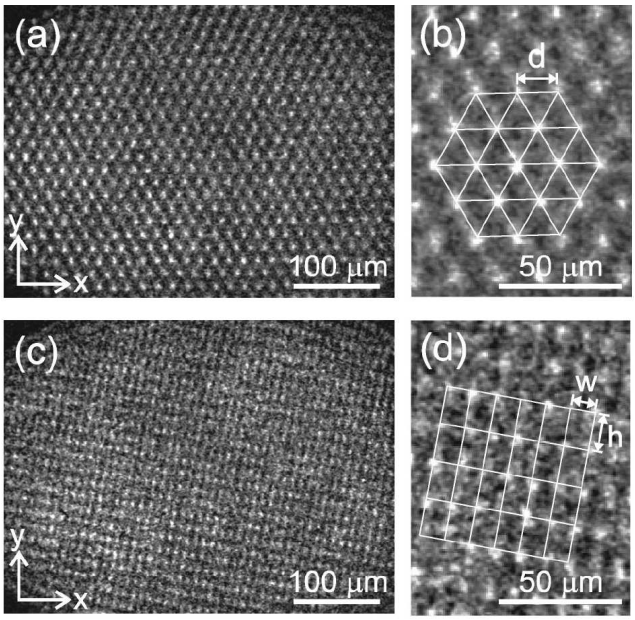

FIGURE 5. Images of a cold ensemble of ∼13 000 ions. (a) Visible hexagonal structures indicating a three-dimensional *bcc* structure. (b) Magnification of a section of (a). (c) Visible rectangular structure likely indicating a slightly distorted *fcc* structure. (d) Magnification of a section of (c).The figure is reproduced from Ref. [17]

OUTLOOK

Experimentally, it is very important in the future to get a better handle on the measurement of the temperature of the ions. In particular, this is necessary before long term statistics of the dynamics in the Coulomb crystals can be compared with theoretical calculations in a meaningful way. Hence, a method to measure the ion temperature through a velocity sensitive stimulated Raman adiabatic passage (STIRAP) process is currently under development in our group. Besides gauging the thermal motion of the ions, this technique will also be able to provide detailed information on the rf field driven micromotion.

Since the energy differences between various metastable crystal structures are relatively small as demonstrated above, it would be interesting to apply periodically induced dipole forces in the form of off-resonant standing wave patterns to control the occurrence of specific structures.

On the theoretical side, MD simulations extending up to $\sim 1s$ in real time would be an ideal way to compare the dynamics observed in the experiments with the simulations. This may though be extremely time consuming, in particular if the rf induced micromotion has to be included. Alternatively, other statistical physics methods, based on e.g. calculations of the density of specific structural states at a given thermal energy might

be more fruitful.

CONCLUSION

Metastable three-dimensional long-range ordering in smaller ion Coulomb crystals confined in rf traps has been discussed. While the long-range ordered structures are found to be consistent with metastable structures found in MD simulations, a significant amount of work lies ahead to fully understand the dynamics of these long-range interacting systems.

REFERENCES

1. A. Rahman, and J. P. Schiffer, *Rev. Mod. Phys.* **54**, 1017 (1982).
2. E. L. Pollock, and J. P. Hansen, *Phys. Rev. A* **8**, 3110 (1973).
3. W. L. Slattery, G. D. Doolen, and H. E. DeWitt, *Phys. Rev. A* **21**, 2087 (1980).
4. A. Rahman, and J. P. Schiffer, *Phys. Rev. Lett.* **57**, 1133 (1986).
5. R. W. Hasse, and J. P. Schiffer, *Ann. Phys.* **203**, 419 (1990).
6. J. P. Schiffer, *Phys. Rev. Lett.* **70**, 818 (1993).
7. J. P. Schiffer, *Phys. Rev. Lett.* **88**, 205003 (2002).
8. D. H. E. Dubin, and T. M. Neil, *Phys. Rev. Lett.* **60**, 511 (1988).
9. J. N. Tan, J. J. Bollinger, B. Jelenkovic, and D. J. Wineland, *Phys. Rev. Lett.* **75**, 4198 (1995).
10. W. M. Itano, J. J. Bollinger, J. N. Tan, B. Jelenković, X.-P. Huang, and D. J. Wineland, *Science* **279**, 686 (1998).
11. T. B. Mitchell, J. J. Bollinger, D. H. E. Dubin, X.-P. Huang, W. M. Itano, and R. H. Baughman, *Science* **282**, 1290 (1998).
12. G. Birkl, S. Kassner, and H. Walther, *Nature* **357**, 310 (1992).
13. M. Drewsen, C. Brodersen, L. Hornekær, J. S. Hangst, and J. P. Schifffer, *Phys. Rev. Lett.* **81**, 2878 (1998).
14. L. Hornekær, N. Kjærgaard, A. M. Thommesen, and M. Drewsen, *Phys. Rev. Lett.* **86**, 1994 (2001).
15. N. Kjærgaard, and M. Drewsen, *Phys. Rev. Lett.* **91**, 095002 (2003).
16. T. Schätz, U. Schramm, and D. Habs, *Nature* **412**, 717 (2001).
17. A. Mortensen, E. Nielsen, T. Matthey, and M. Drewsen, *Phys. Rev. Lett.* **96**, 103001 (2006).
18. M. Drewsen, I. Jensen, J. Lindballe, N. Nissen, R. Martinussen, A. Mortensen, P. Staanum, and D. Voigt, *Int. J. Mass Spectrom.* **229**, 83 (2003).
19. M. Drewsen, and A. Brøner, *Phys. Rev. A* **62**, 045401 (2000).
20. N. Kjærgaard, L. Hornekær, A. Thommesen, Z. Videsen, and M. Drewsen, *Appl. Phys. B* **71**, 207 (2000).
21. A. Mortensen, J. J. T. Lindballe, I. S. Jensen, P. Staanum, D. Voigt, and M. Drewsen, *Phys. Rev. A* **69**, 042502 (2004).
22. R. Blümel, C. Kappler, W. Quint, and H. Walther, *Phys. Rev. A* **40**, 808 (1989).
23. H. Totsuji, T. Kishimoto, C. Totsuji, and K. Tsuruta, *Phys. Rev. Lett.* **88**, 125002 (2002).
24. R. W. Hasse, *J. Phys. B* **36**, 1011 (2003).